NRC Research Press

ARTICLE

Illuminating the photoisomerization of a modified azobenzene single crystal by femtosecond absorption spectroscopy

Kamil M. Krawczyk, Ryan L. Field, Lai Chung Liu, Mingxin Dong, G. Andrew Woolley, and R.J. Dwayne Miller

Abstract: The mechanism of isomerization for azobenzene is a topic still to be completely elucidated. Here, we describe the ultrafast dynamics of a brominated dioxane-methoxy-azobenzene under single crystal conditions by means of femtosecond transient absorption (TA) spectroscopy. Upon excitation with 400 nm light, spectral components with decays of 0.72, 2.9, and >10 ps are observed. The fast components of the system correspond to vibrational cooling of the population on the S_1 excited state, with a decay to a local minimum in the reaction coordinate, followed by a longer evolution to a dark intermediate state prior to relaxing to the ground state, S_0. The long time constant can be used to describe the isomerization process, returning excited population to the ground state. Spectral frequencies observed at 33 and 82 cm^{-1} suggest that both rotation and inversion occur in the system, with a stronger contribution coming from the latter due to a weakened N–N double bond in the excited state. This information provides insight into the structural nature of modified azobenzene systems and sets the stage for future structural studies of the molecule's isomerization dynamics.

Key words: photoisomerization, ultrafast spectroscopy, azobenzene, structural dynamics.

Résumé : Le mécanisme d'isomérisation de l'azobenzène est un sujet qui n'est pas encore complètement élucidé. Dans le présent article, nous décrivons la dynamique ultrarapide d'un dioxane-méthoxyazobenzène bromé en conditions d'observation d'un monocristal au moyen de la spectroscopie d'absorption transitoire femtoseconde. Lorsque le système est excité par la lumière à 400 nm, nous observons des composantes spectrales se désintégrer en 0,72 ps, 2,9 ps et > 10 ps. Les composantes rapides du système correspondent au refroidissement vibrationnel de la population à l'état excité S_1, qui se produit par une décroissance vers un minimum local dans les coordonnées de réaction, suivie par une évolution plus longue vers un état intermédiaire sombre avant de relaxer vers l'état fondamental S_0. La longue constante de temps peut être employée pour décrire le processus d'isomérisation, dans lequel la population excitée retourne à l'état fondamental. Les fréquences spectrales observées à 33 et 82 cm^{-1} laissent supposer que des processus de rotation et d'inversion se produisent dans le système, l'inversion dans une plus large mesure en raison d'une double liaison *N–N* affaiblie dans l'état excité. Ces informations mettent en lumière la nature structurale des systèmes azobenzène modifiés et ouvrent la voie à de futures études structurales de la dynamique d'isomérisation de la molécule. [Traduit par la Rédaction]

Mots-clés : photo-isomérisation, spectroscopie ultrarapide, azobenzène, dynamique structurale.

Introduction

Azobenzene and its derivatives are a popular system for studies of photoisomerization. Their photochromic properties allow them to be commonly employed as control systems for proteins,[1–3] molecular switches,[4,5] and even molecular machines.[6,7] Their applications extend to the solid state, as azobenzene embedded in polymer systems and metal-organic frameworks are capable of isomerization despite steric hinderance.[8–17] Furthermore, the wavelength required to instigate the isomerization process can be modified by phenyl group substitution,[18] including red-shifting to promote absorption at biological wavelengths,[19–21] meaning that azobenzene derivatives can be tailored for their desired application.

Photoexcitation of unmodified azobenzene results from two distinct bands in the absorption spectrum, with a strong $\pi\pi^*$ band in the UV and a weaker $n\pi^*$ band in the visible.[19,22] Substitutions in the phenyl rings of azobenzene can red-shift these bands, allowing access to both bands at lower frequencies of light. Because of the weak, symmetry forbidden $n\pi^*$ transition,[23,24] transient absorption (TA) spectroscopic techniques typically yield low signal to noise (S/N) ratio when performed at these wavelengths. In the liquid state, the concentration may be optimized to increase the signal. In the case of a single crystal, the absorption can be adjusted as a function of thickness of the prepared sample and density of the crystal structure, allowing one to tune this parameter by optimizing the thickness of the sample for the experi-

Received 28 October 2018. Accepted 4 March 2019.

K.M. Krawczyk, R.L. Field, and L.C. Liu. Department of Chemistry, University of Toronto, 80 St. George Street, Toronto, ON M5S 3H6, Canada; Department of Physics, University of Toronto, 60 St. George Street, Toronto, ON M5S 1A7, Canada.
M. Dong. Institute of Neuroregeneration & Neurorehabilitation, Qingdao University, 308 Ningxia Street, Qingdao 266021, China.
G.A. Woolley. Department of Chemistry, University of Toronto, 80 St. George Street, Toronto, ON M5S 3H6, Canada.
R.J.D. Miller. Max Planck Institute for the Structure and Dynamics of Matter, Building 99 (CFEL), Luruper Chaussee 149, 22761 Hamburg, Germany; Department of Chemistry, University of Toronto, 80 St. George Street, Toronto, ON M5S 3H6, Canada; Department of Physics, University of Toronto, 60 St. George Street, Toronto, ON M5S 1A7, Canada.

Corresponding author: R.J. Dwayne Miller (email: dwayne.miller@mpsd.mpg.de).

This paper is part of a Special Issue to honour Professor Ron Steer.

Fig. 1. The mechanisms of *trans*-azobenzene (*t*-AB) to *cis*-azobenzene (*c*-AB) isomerization postulated for azobenzene: (*a*) out-of-plane torsion along the weakened central N–N bond; (*b*) inversion-assisted rotation in plane; (*c*) concerted inversion (hula-twist); and (*d*) inversion in plane.

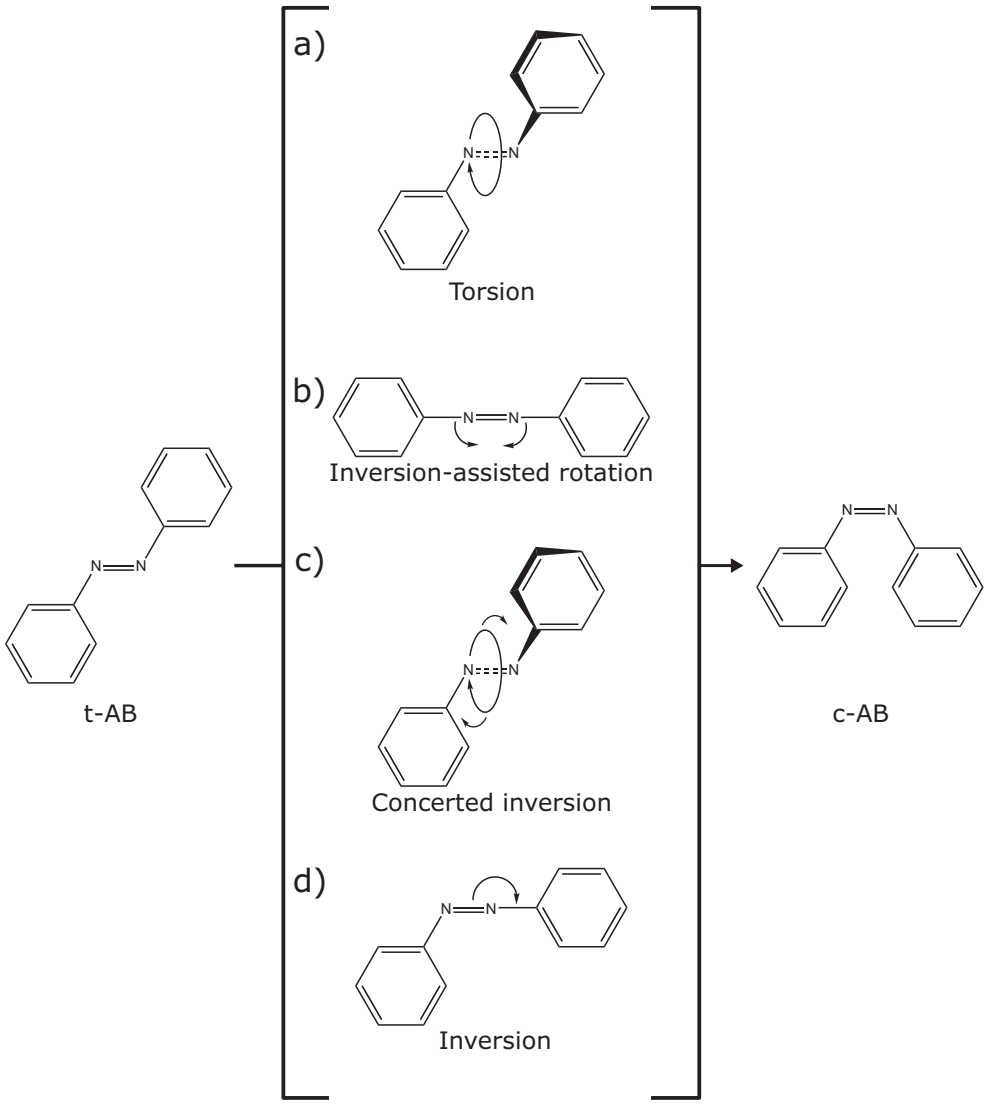

ment. Furthermore, issues with full recovery of the photocycle between excitation pulses fixes the sampling rate for data acquisition, limiting attainable signal to noise levels in femtosecond transient absorption studies of the photochemical processes at hand.

The nature of the photoexcited *trans* to *cis* isomerization mechanism in azobenzene is still a topic of discussion and has been widely discussed in the literature, with many factors such as excitation wavelength, solvent choice, and phenyl ring substitution, affecting the exact mechanism by which isomerization proceeds.[25] Two traditionally proposed isomerization schemes are depicted in Fig. 1: an out-of-plane torsional rotation and an in-plane inversion of a phenyl group.[26–28] The torsional pathway involves the weakening of the central N–N double bond followed by a rotation around the CNNC dihedral angle. The inversion method lacks this weakened N–N double and instead involves an in-plane rotation of the phenyl group along the NNC angle. There is a third and fourth proposed mechanism, the inversion-assisted rotation in-plane,[29,30] and concerted inversion (the hula-twist),[31,32] which stands as combined motions of both torsion and inversion. These differences are reflected in the surfaces of the excited state, and the addition of electron withdrawing or donating groups can affect the potential energy surface barrier height for isomerization by increasing or lowering its value, respectively, leading to differences in which pathway is taken.[25]

Early experiments on the isomerization yield of azobenzene that were modified to be sterically hindered reported identical yields of the *cis* product state regardless of the excitation band used, differing from that of unsubstituted azobenzene.[14,33] For substituted azobenzene, it was proposed that the mechanism of isomerization depended on which band was being excited, with inversion being the predominant motion upon $n\pi^*$ excitation and torsion being the predominant mode upon $\pi\pi^*$ excitation. However, the torsional mode was sterically hindered and thus resulted in equal isomerization yields, unlike in unsubstituted systems, which differed by a factor of 2. Transient absorption studies performed on unsubstituted azobenzene show three exponential decays of 0.2, 1, and 13 ps;[34] these constants were assigned to relaxation from S_n to S_1, vibrational cooling to a minimum, and internal conversion from S_1 to S_0, respectively. Further time-resolved spectroscopic measurements have concluded on similar time constants but with variation in the interpretation of the results,[35–37] commonly concluding that the long-time component observed as being related to vibrational cooling in S_0. More recent work by Quick et al. suggests that the long-lived S_1 intermediate state isomerizes through the hula-twist mechanism due to an

Fig. 2. The chemical structure of 1,2-bis(8-bromo-6-methoxy-2,3-dihydrobenzo[b][1,4]dioxin-5-yl)diazene (BRO-AB) in its *trans* configuration.

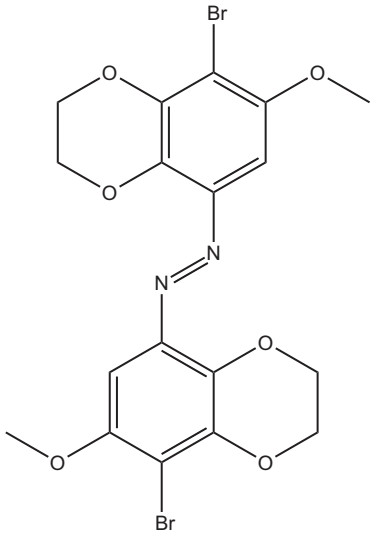

independence of kinetics and the viscosity of the solvent environment.[22] The fast time components of 0.3 and 3 ps were assigned to decay along the S_1 state, with the longer 16 ps time constant being attributed to the transition back to the ground state. Similarly, results from resonant impulsive stimulated Raman spectroscopy (RISRS) show that the isomerization of a modified push–pull azobenzene system also occurs through a multi-dimensional combination of both rotational and inversion coordinates, akin to that of the hula-twist motion.[38] These works stand as the foundation for the results presented here.

In this paper, (1,2-bis(8-bromo-6-methoxy-2,3-dihydrobenzo[b][1,4] dioxin-5-yl)diazene) (herein referred to as BRO-AB, shown in Fig. 2) is studied by broadband probe TA femtosecond spectroscopy to characterize its excited state kinetics, as well as suggest a potential mechanism for isomerization in this substituted system. As BRO-AB is largely substituted and possesses many heavy atoms, it was selected to be able to study the isomerization dynamics in substituted azobenzene and for its increased diffraction quality for future direct structural studies. This work, being performed on a single crystalline sample, sets the foundation for further studies in understanding these mechanisms such as with femtosecond electron diffraction (FED), which allows for the direct visualization of the key modes by direct probing of the changes in real time in the solid state.[39] The femtosecond TA study described here is a necessary prerequisite to determining if the reaction proceeds with the constraints of a crystalline environment and sets the stage for atomically resolving the dynamics of this classic photochemical reaction.

Experimental

Sample and preparation

Crystals of BRO-AB were grown via slow evaporation of the compound dissolved in chloroform over a period of a few weeks. The crystal structure has been previously reported and belongs to $P2_{1/c}$ space group.[40] A DOI link to the crystal structure on the Cambridge Crystallographic Data Centre may be found in the Supplementary data. Thin single crystal sections of the sample were prepared by mounting the sample in a Leica microtome and slicing the (011) face to give 100 nm sections. These thin single crystals were then transferred onto a sapphire window with a thickness of 0.5 mm for spectroscopic measurements.

Experimental setup

The general schematic of the transient absorption pump-probe spectroscopy system is shown in Fig. 3 and is adapted from a previous design.[41] The 800 nm output of a Coherent Micra oscillator and Legend Elite regenerative amplifier is split by a 70:30 beam splitter (BS), generating beams for the pump and probe arms, respectively.

The 800 nm pump arm is frequency doubled by second-harmonic generation (SHG) using a 0.2 mm thick 29.2° cut BBO crystal to generate 400 nm pulses. The final power is controlled by an acousto-optic pulse shaper (AOPS) that also temporally compresses the pulse to the transform limit. The pulse can optionally be characterized by rerouting the beam into a frequency resolved optical gating (FROG) setup. The 800 nm probe arm is used to generate a white light (WL) continuum by white light generation (WLG) in a CaF_2 setup. The path length of both probe and pump beams are matched by propagating the probe arm prior to WLG to ensure that temporal overlap is set.

Both the pump and probe beams are then focused onto the sample with a off-axis parabolic mirror, and into a home-built spectrometer based on the Czerny–Turner design, and into a calibrated CCD array for detection with sub-nanometer spectral resolution. The beam sizes at the sample position are 90 and 30 μm full width at half maximum (FWHM) for the pump and the probe, respectively. The pump fluence was set to be in the linear pumping regime to prevent damage or non-linear effects.

Analysis of transient absorption data

Data acquired were first corrected for group velocity dispersion (GVD) for a blank sapphire window, correcting for variation in $t = 0$ across all wavelengths probed. By fitting the corrected self-phase modulation curve of the blank, the instrument response function (IRF) was determined to be 68 ± 5 fs FWHM. The corrected data were then used in a global analysis (GA) fit by modelling an exponential decay and three components from singular value decomposition (SVD). Further details on the analysis of the data are detailed here.[41]

Analysis of residuals

The residuals depict any leftover oscillatory components or cross-phase modulation (CPM) obscured by the exponential population dynamics. Here, the residuals were calculated by taking the difference between the raw data and the GA fit. The data were reconstructed with the same number of SVD components as used in the GA fit prior to taking the difference. The two-dimensional residuals map is shown in Supplementary Fig. S1 and a few representative traces at select wavelengths are shown in Supplementary Figs. S2–S4. For each wavelength of the residuals, Welch's method, which relies on a Fourier transform, is used to estimate the power of the signal at distinct frequencies. The signal was then integrated for overall wavelengths; then, the peak positions and standard deviation were calculated by fitting a Gaussian to each prominent peak.

Results and discussion

Dynamics

The resulting TA scans after GVD correction and GA for single crystal BRO-AB are shown in Fig. 4. The data were taken over a range from –1 to 10 ps with 25 fs timesteps, using 57 fs, 400 nm pump pulses. The polarization of the pump beam was set to maximize 400 nm absorption, with the probe beam being circularly polarized. It should be noted that the pump scatter was removed prior to analysis by only fitting regions > 400 nm in the raw GVD corrected data. The absorption spectrum for a 100 nm crystal is shown in Fig. 5, showing both suggested excitation bands in the BRO-AB single crystal.

The decay associated spectra (DAS) from GA and their time constants are presented below in Fig. 6. Dynamics not modelled in the

Fig. 3. Schematic of the TA spectroscopy instrument. The output beam from the regenerative amplifier is split by a 30:70 BS (BS1) into the pump and probe arm. The pump arm is doubled by SHG into 400 nm and passed through the AOPS prior to the retroreflector (RR) delay arm. The probe arm passes through a 10:90 BS (BS2) and is then used to prepare a WL continuum. Both the pump and the probe are focused onto the sample by off-axis parabolic mirrors, with the residual pump being blocked and the probe being sent to a spectrometer (SP).

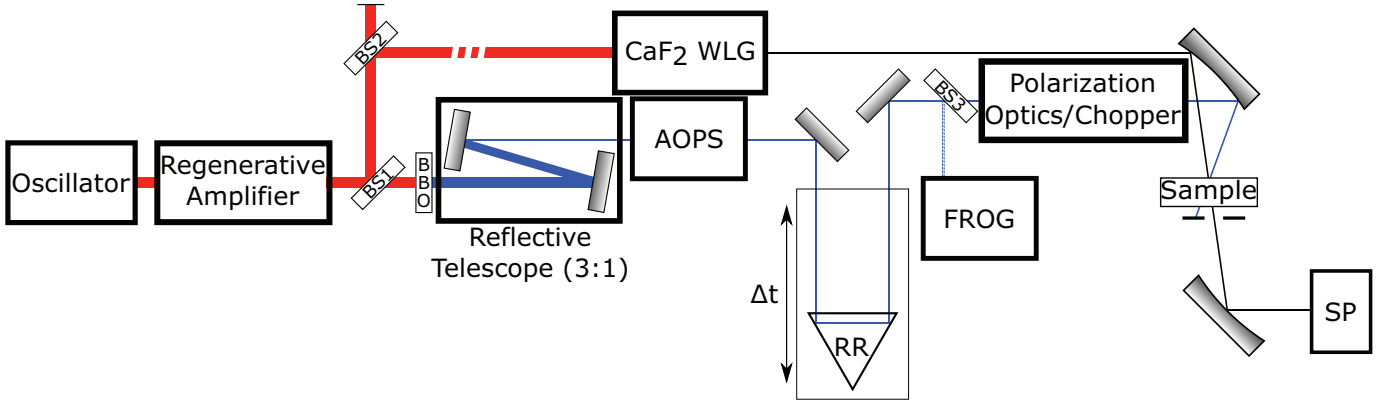

Fig. 4. TA scans of single crystal BRO with pump scatter removed: (*a*) the GVD corrected data and (*b*) the results of the GA fit applied to the GVD corrected data. Bleach and excited state absorption (ESA) signals are observed as negative and positive changes in absorbance, respectively.

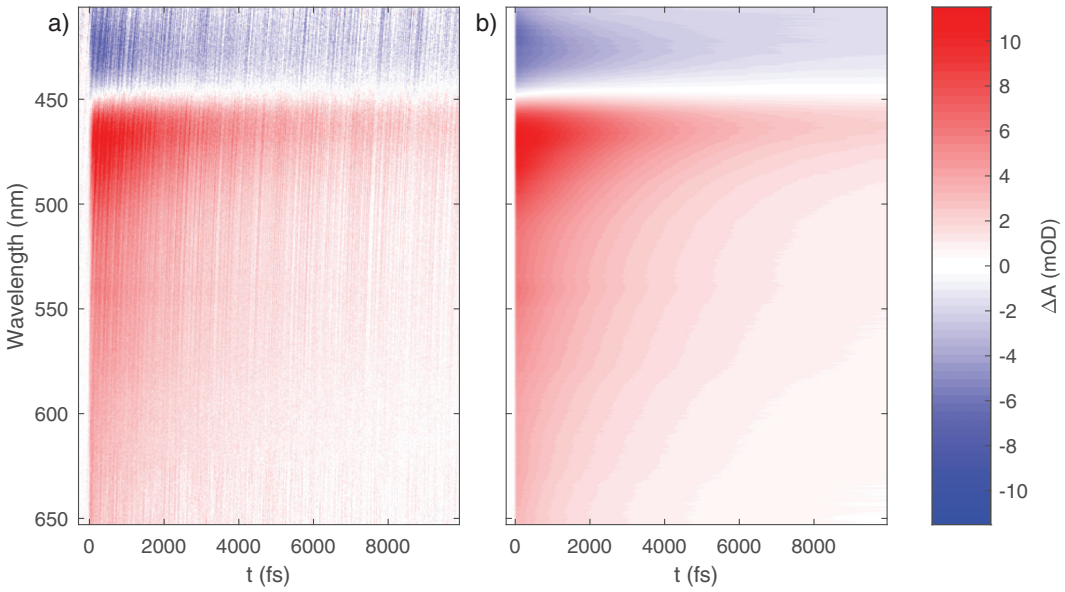

GA such as oscillations can be resolved in the residuals of the fit and will be discussed below. Three DAS and their respective time constants were fitted to the data, with two short time components of 0.72 ps and 2.9 ps, as well as a time constant that exceeds the length of the measured data and is thus ill-resolved. For this work, the time constant is considered to be >10 ps, but consistent within the fit error to previously reported values. These time constants are consistent with results previously reported in literature for unsubstituted and modified systems studied in the solution phase such as 4-nitro-4′-dimethylaminoazobenzene (NDAB).[22,34,35,38,42]

Here, we interpret the short spectral component, with associated time constant 0.72 ps, as vibrational cooling along the S_1 state to a local minimum. Wavelengths > 500 nm in the DAS show positive signal attributed to this time constant, consistent with an overall red shift and narrowing of positive differential absorption (DA) signal for wavelengths between 460 and 650 nm, as seen in the two-dimensional GA fit plot in Fig. 4. Similarly, the other short decay component, at 2.9 ps, in the same >500 nm wavelength regime, has a positive, spectrally narrowing signal in the same GA fit plot. This is also suggestive of further vibrational cooling and is consistent with the literature in being assigned as another decay into a second minimum along the S_1 manifold. Evidence supporting this can also be seen in the two-dimensional GA plot as a similar narrowing of positive signal between 460 and 500 nm on the order of the given time constant. In static solution phase, a blue shift of the absorption spectrum is seen after continuous wave (CW) laser irradiation is used to form the *cis* photoproduct.[40] A difference in the absorption spectra of a dark-adapted sample and an irradiated sample shows a clear region of decreased absorption isosbestic to a region of increased absorption. This feature can be seen in the GA fit alongside that of vibrational cooling, providing supporting evidence that the *cis* product of BRO-AB has been formed. This is made more evident in the long-lived transient DAS for the 2.9 ps and >10 ps components, showing nearly identical features to the difference in static absorption spectra.

The long time constant, which was found to have the same order of magnitude as the longer time scales reported in literature, cannot be resolved exactly due to the nature of the global fit and the short time range of the acquired data. However, this decay can be presumed to be the recovery of population from the S_1 state minimum back to the fully relaxed ground states.[22]

Fig. 5. The absorption spectrum of a 100 nm thick single crystal sample, showing key peaks and their attributed excitation pathways.

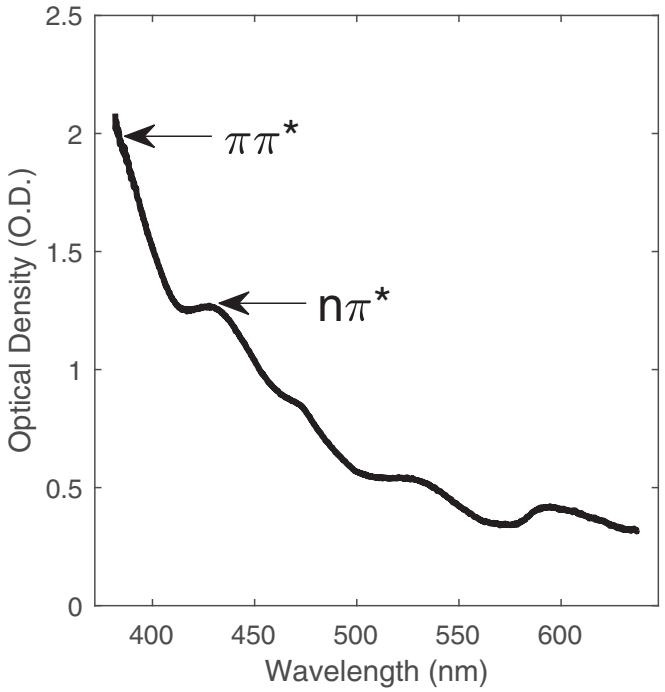

Fig. 6. The DAS resulting from GA fit of the GVD corrected data and their respective time constants.

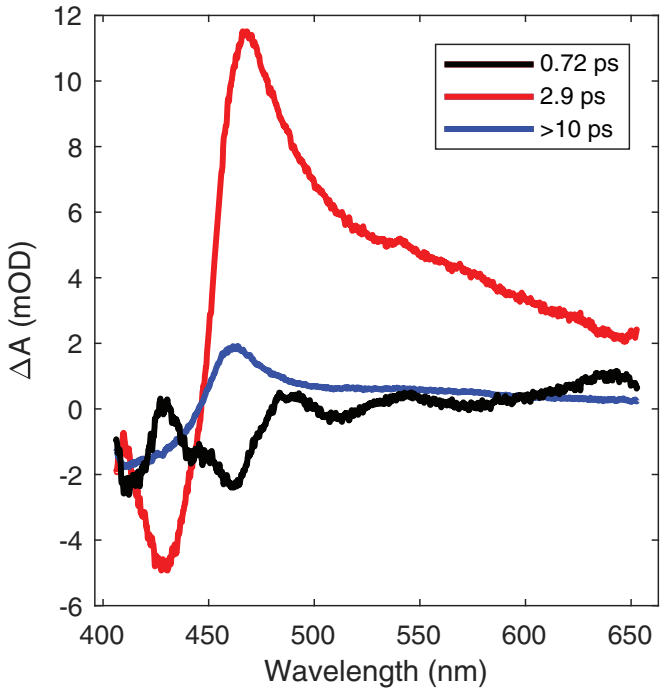

We have assigned both the weak $n\pi^*$ and strong $\pi\pi^*$ bands to the absorption spectrum of the single crystal (Fig. 5). Compared with the UV–vis absorption spectrum of the *trans* isomer in solution phase,[40] there is a red shift of these peaks likely due to a lack of solvent interactions in the solid state. Thus, excitation at 400 nm occurs at a point crossing between both bands in the solid state.

Excitation along the stronger $\pi\pi^*$ band results in a transition from the ground state to S_n, an excited manifold higher in energy than that of the S_1 manifold, the state accessed during excitation along the $n\pi^*$ band. A decay from S_n to S_1 is expected to involve approximately half of the excited population based on the relative absorption into the $\pi\pi^*$ and $n\pi^*$ bands at the excitation wavelength. The $\pi\pi^*$ population decays over 0.1–0.2 ps, followed by a cascade down to the S_1 minima, similar to that of excitation directly to S_1.[22] The GA model is unable to resolve a faster time component due to the inherently low S/N observed at the excitation powers used; it may also be mixed in or obscured in the CPM signal. Evidence supporting excitation along $\pi\pi^*$ can be seen in the cross sections of the TA data taken at short time intervals, as seen in Fig. 7. The ESA seen at ~470 nm first increases in magnitude from 0.1 to 0.2 ps and then continually decreases over time.

From these results, the following overall scheme is suggested: upon photoexcitation with 400 nm light, population excitation to the S_n state occurs, as well as some to the S_1 state. From this point, a fast, sub-0.3 ps evolution occurs to the S_1 state, followed by a 0.72 ps decay to a local minimum and a longer 2.9 ps decay to the bottom of the S_1 well. These decays represent vibrational cooling during this process, as is made evident by the spectral narrowing of the ESA in conjunction with the decay rates. Lastly, a >10 ps decay occurs back to the ground state, S_0, of the *trans* isomer and the ground state of the *cis* photoproduct, by crossing through a CI with an energetic barrier in the excited state surface as shown in Fig. 8. It is this barrier to forming the CI in the excited state that results in the long >10 ps dynamics involved in the CI crossing to the *trans* ground state and *cis* photoproduct surface. The branching ratio for this process is reported as being on the order of 20% in solution phase unsubstituted azobenzene and is assumed to be similar for BRO-AB based on similar magnitudes for the difference spectra.[22] However, future studies to accurately determine the quantum yield of the photoisomerization process in BRO-AB will need to be performed. Contribution from excitation to the S_n state is weak and therefore difficult to confirm, but evidence supporting excitation to the state is observed in the DA slices over the course of the first 300 fs. This overall decay pathway is depicted in Fig. 8.

Oscillations in residuals

The residuals of the fit were calculated by taking the difference between the GVD corrected data and the GA fit data, using the same number of components to represent the corrected data as were used in the GA analysis. A Welch spectral power estimate was performed and integrated for all wavelengths, resulting in a description of the dominant frequencies observed in the residuals (Fig. 9).

RISRS in conjunction with DFT calculations have been performed on NDAB in the solution phase to elucidate key modes observed upon photoexcitation.[38] Modes at ~15 cm^{-1} and ~50 cm^{-1} correspond to a weak torsional and strong inversion mode, respectively, indicating a fast in-plane motion with a slower torsional mode that compensates for phenyl–phenyl steric effects upon isomerization; these modes describe the excited state *trans* to *cis* photoisomerization reaction coordinate of NDAB in the Franck–Condon (FC) region. Resonance Raman performed on a mixture of *trans* and *cis* unsubstituted azobenzene in the liquid indicate low frequency bands at 275 cm^{-1}.[43] It was found that these modes would have an increased intensity when the mixture predominantly contained the *cis* isomer and are attributed to torsional modes having increased FC displacements in the excited state.

NDAB falls into the category of push-pull azobenzene systems, with the dimethylamino group donating electronic density and the nitro group withdrawing it from the π system. In contrast, the system we study is more aptly described as a pull–pull system, as it contains two identical electron withdrawing groups on opposite phenyl groups. Thus, in the framework of BRO-AB, the central

Fig. 7. Early evolution of DA spectra taken at 0.1, 0.2, 0.3, and 1 ps time slices. Here, an initial increase and subsequent decrease is observed in two ESA features over the period of 200 fs, with some interference affecting the signal amplitude due to CPM at 0.1 ps. These dynamics and spectral trends are similar with results seen upon $\pi\pi^*$ excitation of *trans*-azobenzene in solution.[22] Spectra are smoothed slightly using a rolling average over 20 data points.

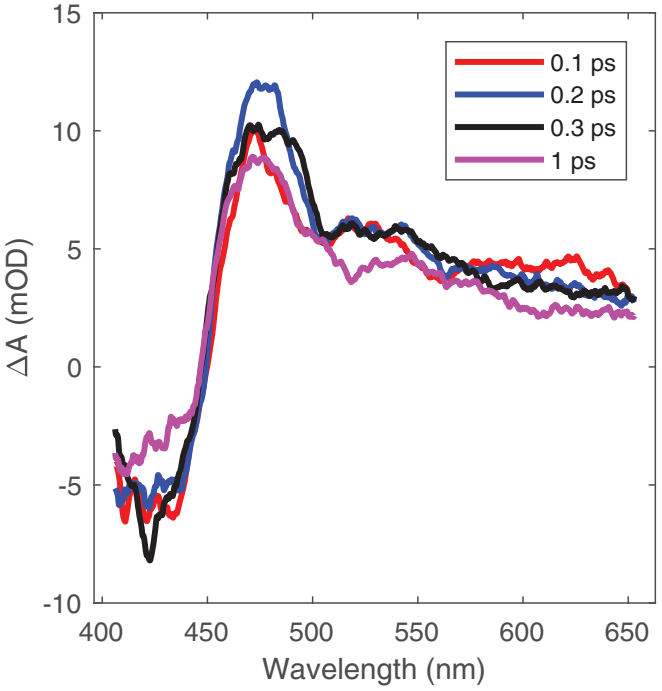

Fig. 8. Proposed reaction coordinate energy schematic along a combined torsion/inversion hula-twist isomerization pathway for excitation along $n\pi^*$ and $\pi\pi^*$ pathways of BRO-AB with associated decay constants. The dotted lines represent vibrational nonadiabatic coupling, forming a CI at indeterminate coordinates.

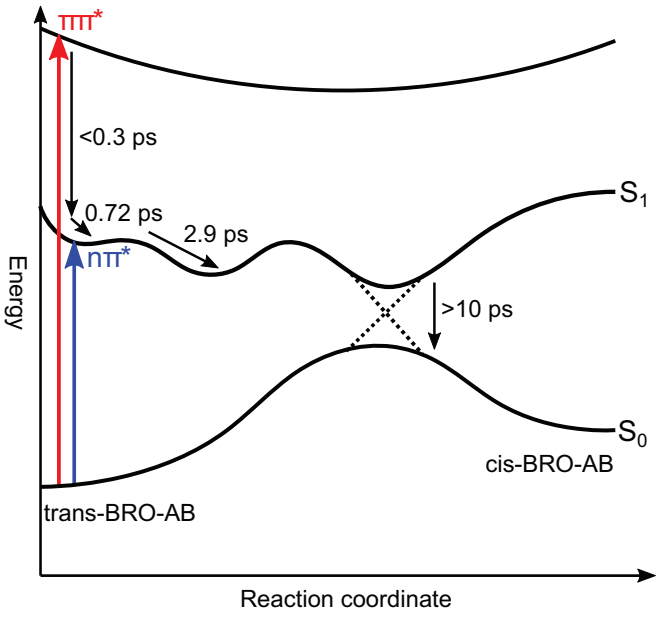

N–N double bond is likely weakened due to having electron density withdrawn from the π system.

From the Welch power density spectrum, four significant frequencies can be extracted at 33 ± 24, 82 ± 28, 135 ± 27, and 284 ± 15 cm^{-1}. Another frequency is seen at 333 ± 17 cm^{-1}, but this is closer to the noise floor. The extracted frequencies are difficult to assign to specific vibrational modes, as no appropriate studies have yet been performed on BRO-AB. The modes observed at 33 and 82 cm^{-1} show similarity within their deviation to the key low frequency modes observed in NDAB. These contribute predominantly in the bleach band seen in the GA fit presented in Fig. 4. We tentatively assign these modes to the torsion and inversion, respectively, based on their near proximity to these previously assigned modes for NDAB.[38] The mode at 284 ± 15 cm^{-1} is similar within its deviation to the torsional mode observed in predominantly *cis* liquid state azobenzene. This mode contributes predominantly in the region of increased absorption seen in the GA fit in Fig. 4. We tentatively assign this mode to the torsional mode along the excited state surface.

The uncertainty in the extracted modes presented can make it difficult to clearly assign them to specific vibrational modes without appropriate theory and additional spectroscopic studies on BRO-AB. Furthermore, the observed wavelength range is limited, and such integration does not reliably cover the full bleach portion; thus, oscillations that may be present at wavelengths < 400 nm are not measured and cannot be included in the integration. There is difficulty in determining which mode is more significant when comparing the amplitudes of these two peaks. The sample is cut along the (011) plane. In this orientation, the molecules in the unit cell are mostly orthogonal with respect to the incoming probe beam. A thorough understanding of the transition dipole orientation is needed to determine the relative contribution of each observed mode to the isomerization process based solely on spectral amplitudes.

Finally, the observed modes alone do not unambiguously confirm the presence of the *cis* photoproduct without further studies. However, when coupled with the shape of the differential absorption spectra as additional evidence for isomerization, they provide insight in to the predominant modes seen when *cis* photoproduct formation occurs in the BRO-AB single crystal. The degree to which these modes are involved in the reaction requires future direct structural studies.

We suggest that, in the case of a pull–pull system such as BRO-AB, torsional modes may contribute more significantly to the isomerization process. This motion, in addition to modes related to inversion, would give rise to an overall hula-twist motion. It is likely that the weakened N–N bond and the steric hinderance in effect in the crystal environment play a role in differentiating the modes observed upon isomerization. However, to fully understand the key atomic motions related to these modes and their role in photoisomerization, a more direct structural probe must be used such as FED. In FED, one is able to study structural changes in solid state materials directly, as it combines the structural elucidation of X-ray and electron diffraction with the time resolution of ultrafast spectroscopic techniques.[39] This work serves as a precursor to better understanding the dynamics at play by investigating the excited state dynamics of single crystal BRO-AB. This information is critical for studying the sample with FED to both confirm that there is evidence for photoinduced reactions and provide excited state dynamics. This combined information will correlate the electronic and nuclear degrees of freedom. We have found that single crystal BRO-AB exhibits similar excitation dynamics and differential spectral signatures to that of solution phase studies. This indicates that, despite being under single crystal conditions, the system is poised to photoisomerize even with lattice constraints, as they evidently are a relatively small perturbation on the problem in comparison to the localized forces on the excited state surface that drive the isomerization.

Fig. 9. (*a*) The Welch power density spectrum for all wavelengths; (*b*) the integrated Welch power density spectrum for all wavelengths. Significant oscillatory frequencies are observed at 33 ± 28, 82 ± 28, and 284 ± 15 cm^{-1}, with two weak peaks present at 135 ± 27 and 333 ± 17 cm^{-1}.

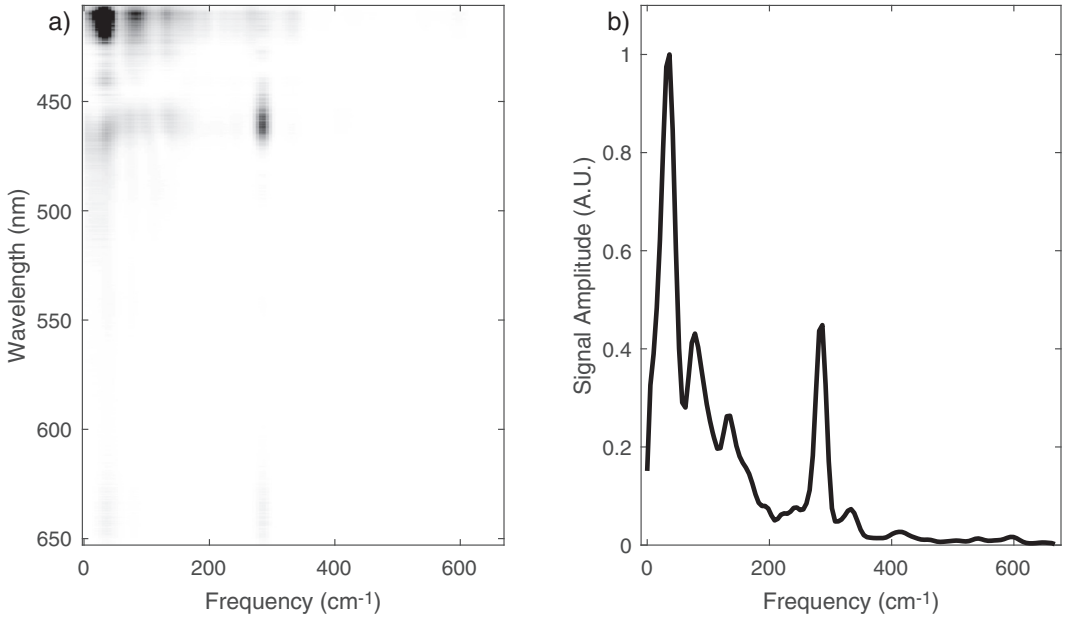

Conclusion

Photoexcitation of BRO-AB with 400 nm pump pulses excites both the $\pi\pi^*$ and $n\pi^*$ pathways, which leads to a triexponential decay with time constants 0.72, 2.9, and >10 ps. Excitation to the higher energy S_2 state by the $\pi\pi^*$ pathway is observed by the increase and subsequent decrease of the ESA observed in the DA spectra over the course of the first 300 fs, although it is not resolvable by the GA fit used. The shorter time constants reflect vibrational cooling to minima along the S_1 state, followed by a longer decay to the S_0 ground state *trans* and *cis* photoproduct states. These dynamics are virtually identical to those observed in solution, where the isomerization process has been well characterized. Oscillations observed in the residuals of the data show strong resonances at 33, 82, and 284 cm^{-1}, and in relation to solution phase studies, suggest that the isomerization pathway of BRO-AB includes contributions from both the rotation and inversion pathway. Confirmation of whether these modes are reactive or simply spectator modes will be reserved for future structural studies. This study provides the groundwork for FED studies to atomically resolve the passage through the CI, a key requirement for fully understanding the photochemistry and the key reaction modes directing photoisomerization in azobenzene.

Supplementary data

Supplementary data are available with the article through the journal Web site at http://nrcresearchpress.com/doi/suppl/10.1139/cjc-2018-0461.

Acknowledgements

We acknowledge NSERC and the Max Planck Society for their financial support. KMK acknowledges the School of Graduate Studies for their support with the Ontario Graduate Scholarship. We also thank Jordan Wentzell for his technical help with the microtome and Dr. Yifeng Jiang for his guidance.

References

(1) Mart, R. J.; Allemann, R. K. *Chem. Commun.* **2016**, *52* (83), 12262. doi:10.1039/C6CC04004G.
(2) Luo, J.; Samanta, S.; Convertino, M.; Dokholyan, N. V.; Deiters, A. *ChemBioChem* **2018**, *19*, 2178. doi:10.1002/cbic.201800226.
(3) Müller, A.; Lindhorst, T. K. *Eur. J. Org. Chem.* **2016**, *2016* (9), 1669. doi:10.1002/ejoc.201600136.
(4) Kumar, A. S.; Ye, T.; Takami, T.; Yu, B. C.; Flatt, A. K.; Tour, J. M.; Weiss, P. S. *Nano Lett.* **2008**, *8* (6), 1644. doi:10.1021/nl080323+.
(5) Zhang, C.; Du, M. H.; Cheng, H. P.; Zhang, X. G.; Roitberg, A. E.; Krause, J. L. *Phys. Rev. Lett.* **2004**, *92* (15), 158301. doi:10.1103/PhysRevLett.92.158301.
(6) Norikane, Y.; Tamaoki, N. *Org. Lett.* **2004**, *6* (15), 2595. doi:10.1021/ol049082c.
(7) Shinkai, S.; Shigematsu, K.; Kusano, Y.; Manabe, O. *J. Chem. Soc., Perkin Trans. 1* **1981**, 3279. doi:10.1039/P19810003279.
(8) Brown, J. W.; Henderson, B. L.; Kiesz, M. D.; Whalley, A. C.; Morris, W.; Grunder, S.; Deng, H.; Furukawa, H.; Zink, J. I.; Stoddart, J. F.; Yaghi, O. M. *Chem. Sci.* **2013**, *4* (7), 2858. doi:10.1039/c3sc21659d.
(9) Wang, Z.; Heinke, L.; Jelic, J.; Cakici, M.; Dommaschk, M.; Maurer, R. J.; Oberhofer, H.; Grosjean, S.; Herges, R.; Bräse, S.; Reuter, K.; Wöll, C. *Phys. Chem. Chem. Phys.* **2015**, *17* (22), 14582. doi:10.1039/C5CP01372K.
(10) Modrow, A.; Zargarani, D.; Herges, R.; Stock, N. *Dalton Trans.* **2012**, *41* (28), 8690. doi:10.1039/c2dt30672g.
(11) Modrow, A.; Zargarani, D.; Herges, R.; Stock, N. *Dalton Trans.* **2011**, *40* (16), 4217. doi:10.1039/c0dt01629b.
(12) Heinke, L.; Cakici, M.; Dommaschk, M.; Grosjean, S.; Herges, R.; Bräse, S.; Wöll, C. *ACS Nano* **2014**, *8* (2), 1463. doi:10.1021/nn405469g.
(13) Yager, K. G.; Barrett, C. J. *J. Photochem. Photobiol., A* **2006**, *182* (3), 250. doi:10.1016/j.jphotochem.2006.04.021.
(14) Rau, H.; Yu-Quan, S. *J. Photochem. Photobiol., A* **1988**, *42* (2–3), 321. doi:10.1016/1010-6030(88)80075-3.
(15) Parker, R. M.; Gates, J. C.; Rogers, H. L.; Smith, P. G. R.; Grossel, M. C. *J. Mater. Chem.* **2010**, *20* (41), 9118. doi:10.1039/c0jm01334j.
(16) Qin, C.; Feng, Y.; An, H.; Han, J.; Cao, C.; Feng, W. *ACS Appl. Mater. Interfaces* **2017**, *9* (4), 4066. doi:10.1021/acsami.6b15075.
(17) Akiyama, H.; Fukata, T.; Yamashita, A.; Yoshida, M.; Kihara, H. *J. Adhes.* **2017**, *93* (10), 823. doi:10.1080/00218464.2016.1219255.
(18) Forber, C. L.; Kelusky, E. C.; Bunce, N. J.; Zerner, M. C. *J. Am. Chem. Soc.* **1985**, *107* (21), 5884. doi:10.1021/ja00307a009.
(19) Dong, M.; Babalhavaeji, A.; Hansen, M. J.; Kálmán, L.; Woolley, G. A. *Chem. Commun.* **2015**, *51*, 12981. doi:10.1039/C5CC02804C.
(20) John, A. A.; Ramil, C. P.; Tian, Y.; Cheng, G.; Lin, Q. *Org. Lett.* **2015**, *17* (24), 6258. doi:10.1021/acs.orglett.5b03268.
(21) Dong, M.; Babalhavaeji, A.; Samanta, S.; Beharry, A. A.; Woolley, G. A. *Acc. Chem. Res.* **2015**, *48* (10), 2662. doi:10.1021/acs.accounts.5b00270.
(22) Quick, M.; Dobryakov, A. L.; Gerecke, M.; Richter, C.; Berndt, F.; Ioffe, I. N.; Granovsky, A. A.; Mahrwald, R.; Ernsting, N. P.; Kovalenko, S. A. *J. Phys. Chem. B* **2014**, *118* (29), 8756. doi:10.1021/jp504999f.
(23) Siampiringue, N.; Guyot, G.; Monti, S.; Bortolus, P. *J. Photochem.* **1987**, *37* (1), 185. doi:10.1016/0047-2670(87)85039-6.
(24) Bortolus, P.; Monti, S. *J. Phys. Chem.* **1979**, *83* (6), 648. doi:10.1021/j100469a002.
(25) Bandara, H. M. D.; Burdette, S. C. *Chem. Soc. Rev.* **2012**, *41* (5), 1809. doi:10.1039/C1CS15179G.
(26) Tiago, M. L.; Ismail-Beigi, S.; Louie, S. G. *J. Chem. Phys.* **2005**, *122* (9), 094311. doi:10.1063/1.1861873.

(27) Tiberio, G.; Muccioli, L.; Berardi, R.; Zannoni, C. *ChemPhysChem* **2010**, *11* (5), 1018. doi:10.1002/cphc.200900652.
(28) Cembran, A.; Bernardi, F.; Garavelli, M.; Gagliardi, L.; Orlandi, G. *J. Am. Chem. Soc.* **2004**, *126* (10), 3234. doi:10.1021/ja038327y.
(29) García-Amorós, J.; Velasco, D. *Beilstein J. Org. Chem.* **2012**, *8*, 1003. doi:10.3762/bjoc.8.113.
(30) Dou, Y.; Hu, Y.; Yuan, S.; Wu, W.; Tang, H. *Mol. Phys.* **2009**, *107* (2), 181. doi:10.1080/00268970902769497.
(31) Böckmann, M.; Doltsinis, N. L.; Marx, D. *J. Phys. Chem. A* **2010**, *114* (2), 745. doi:10.1021/jp910103b.
(32) Jiang, C.-W.; Xie, R.-H.; Li, F.-L.; Allen, R. E. *J. Phys. Chem. A* **2011**, *115* (3), 244. doi:10.1021/jp107991a.
(33) Rau, H.; Lueddecke, E. *J. Am. Chem. Soc.* **1982**, *104* (6), 1616. doi:10.1021/ja00370a028.
(34) Lednev, I. K.; Ye, T.-Q.; Matousek, P.; Towrie, M.; Foggi, P.; Neuwahl, F. V. R.; Umapathy, S.; Hester, R. E.; Moore, J. N. *Chem. Phys. Lett.* **1998**, *290* (1–3), 68. doi:10.1016/S0009-2614(98)00490-4.
(35) Fujino, T.; Tahara, T. *J. Phys. Chem. A* **2000**, *104* (18), 4203. doi:10.1021/jp992757m.
(36) Fujino, T.; Arzhantsev, S. Y.; Tahara, T. *J. Phys. Chem. A* **2001**, *105* (35), 8123. doi:10.1021/jp0110713.
(37) Satzger, H.; Root, C.; Braun, M. *J. Phys. Chem. A* **2004**, *108* (30), 6265. doi:10.1021/jp049509x.
(38) Hoffman, D. P.; Ellis, S. R.; Mathies, R. A. *J. Phys. Chem. A* **2013**, *117* (45), 11472. doi:10.1021/jp408470a.
(39) Miller, R. J. D. *Annu. Rev. Phys. Chem.* **2014**, *65* (1), 583. doi:10.1146/annurev-physchem-040412-110117.
(40) Dong, M.; Babalhavaeji, A.; Collins, C. V.; Jarrah, K.; Sadovski, O.; Dai, Q.; Woolley, G. A. *J. Am. Chem. Soc.* **2017**, *139* (38), 13483. doi:10.1021/jacs.7b06471.
(41) Field, R.; Liu, L. C.; Gawelda, W.; Lu, C.; Miller, R. J. D. *Chem. - Eur. J.* **2016**, *22* (15), 5118. doi:10.1002/chem.201600374.
(42) Hoffman, D. P.; Mathies, R. A. *Phys. Chem. Chem. Phys.* **2012**, *14* (18), 6298. doi:10.1039/c2cp23468h.
(43) Stuart, C. M.; Frontiera, R. R.; Mathies, R. A. *J. Phys. Chem. A* **2007**, *111* (48), 12072. doi:10.1021/jp0751460.